Novel one-pot green synthesis of graphene in aqueous medium under microwave irradiation using regenerative catalyst and study of its electrochemical properties

Journal:	*New Journal of Chemistry*
Manuscript ID:	NJ-ART-08-2014-001359.R1
Article Type:	Paper
Date Submitted by the Author:	07-Oct-2014
Complete List of Authors:	B, Subramanya; NITK, Chemistry Bhat, D. Krishna; NITK, Department of Chemistry

Novel one-pot green synthesis of graphene in aqueous medium under microwave irradiation using regenerative catalyst and study of its electrochemical properties

Badrayyana Subramanya and Denthaje Krishna Bhat*

Department of Chemistry

National Institute of Technology Karnataka, Surathkal, Mangalore-575 025, India.

*Corresponding author: Tel: +91-824-2473202; Fax: +91-824-74033/2474082

E-mail: denthajekb@gmail.com, kishan@nitk.edu.in

Table of Contents (TOC)

High throughput synthesis of superior quality graphene by a unified green approach for high performance supercapacitors.

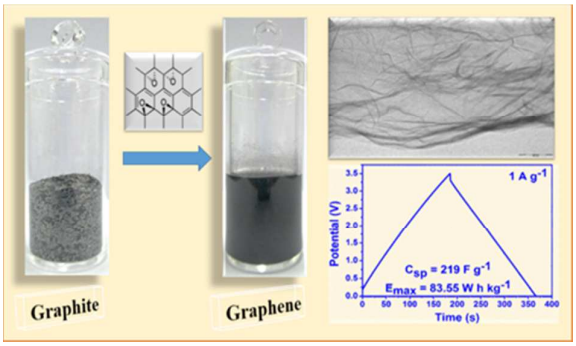

Novel one-pot green synthesis of graphene in aqueous medium under microwave irradiation using regenerative catalyst and study of its electrochemical properties

Badrayyana Subramanya and Denthaje Krishna Bhat*

Department of Chemistry

National Institute of Technology Karnataka, Surathkal, Mangalore-575 025, India.

*Corresponding author: Tel: +91-824-2473202; Fax: +91-824-74033/2474082

E-mail: denthajekb@gmail.com, kishan@nitk.edu.in

Abstract

In this work we report an economic, eco-friendly, high yielding and facile one-pot method for the large scale synthesis of few layer graphene (FLG) nanosheets directly from graphite in aqueous medium using a regenerative catalyst, sodium tungstate. This method is fast and makes use of environment friendly chemicals and microwave radiation. The as-synthesized FLG nanosheets are characterized by field emission scanning electron microscopy (FESEM), transmission electron microscopy (TEM), X-ray diffraction (XRD), Raman spectroscopy, X-ray photoelectron spectroscopy (XPS) and Brunauer-Emmett-Teller (BET) surface area analysis. Raman analysis indicates the as-synthesized graphene is bilayered with a smaller domain size of 3.9 nm which is responsible for higher specific surface area of FLG nanosheets (1103.62 m^2 g^{-1}). Moreover, XPS analysis of FLG nanosheets show a high C:O ratio (~9.6) which is best among the graphene prepared from green chemicals. The electrochemical performance of as-synthesized FLG nanosheets is analysed by cyclic voltammetry (CV), chronopotentiometry and electrochemical impedance spectroscopy (EIS) in neat 1-ethyl-3-methylimidazolium tetrafluoroborate ($EMIMBF_4$) electrolyte. The superior capacitive performance with large capacitance (219 F g^{-1}), high energy density (83.56 W h kg^{-1}) and excellent cyclability (3000 cycles) exhibited by these graphene nanosheets makes it an excellent candidate for suercapacitor material.

Introduction

Graphene, a one-atom thick sheet of carbon atoms in a closely packed two-dimensional honeycomb lattice, has gained extensive consideration in recent years due to its unique properties.[1-6] Due to the fast charge carrier mobility, high mechanical strength and large theoretical surface area of graphene they find potential applications in the field of energy storage.[7, 8] Numerous physical and chemical methods have been developed to prepare high quality graphene since its discovery in 2004. High quality monolayer graphene can be obtained by mechanical exfoliation of graphite[2], epitaxial growth[9, 10], chemical vapour deposition (CVD)[11], thermal exfoliation[12] and liquid-phase exfoliation of graphite[13-15] have been reported. However, all of these methods either fail to achieve complete exfoliation to individual graphene sheets or the yield is very low. Chemical exfoliation of graphite and subsequent reduction is scalable and economical but require multi-step processes including separation and purification steps, generate large amounts of waste and only produce graphene with a relatively low C:O ratio which indicates a disruption in its long range order and limit its practical application.[16-18] The extensive usage of reducing agents in this approach may have detrimental effect on the environment. Recently, the direct electrochemical exfoliation of graphite into graphene nanosheets has been reported.[19, 20] However, these methods have major disadvantages, including the requirement of costly chemicals such as ionic liquids and/or hazardous reagents such as phosphoric acid, lithium perchlorate etc, high voltages, low quality, multilayer graphene formation and difficulty in scaling up. However, a unified green approach for the one-pot synthesis of graphene in large scale using microwave radiation has not been reported yet.

Herein, we report a microwave based facile one-pot method for the large-scale synthesis of graphene sheets directly from graphite in aqueous medium. The major benefits of present work include: fast, green and no usage of toxic solvents, direct conversion of graphite into graphene, regeneration (reoxidation) of catalyst in the reaction cycle with water as the only by-product of the reaction. Direct high yield conversion of graphite to graphene is possible because effective intercalation and exfoliation is possible under microwave irradiation as the precursor, graphite and the reaction medium, water are good microwave absorbers. The microwave radiation heats the reactants through selective transfer of energy resulting in multiple breaking of graphite by repeated oxidation reactions aided by the catalyst. Meanwhile there is a simultaneous increase in self-generated pressure inside the sealed reaction vessel aiding in exfoliation of intercalated graphite. This results in shortening of the reaction time from several hours to a few minutes with an effective energy economy. The as-synthesized graphene was studied as an electrode material for supercapacitors in neat $EMIMBF_4$ electrolyte. The high surface area coupled with ideal bimodal pore size distribution of as-synthesized graphene nanosheets results in a high specific capacitance of 219 F g^{-1} and an energy density of 83.56 W h kg^{-1}.

Experimental

Materials

Graphite flakes (CAS Number 7782-42-5), sodium tungstate dihydrate (CAS Number 10213-10-2), 1-ethyl-3-methylimidazolium tetrafluoroborate (CAS Number 143314-16-3), nafion (CAS Number 31175-20-9) and isopropanol (CAS Number 67-63-0) were procured from Sigma Aldrich. Hydrogen peroxide (CAS Number 7722-84-1) was procured from Merck India.

Synthesis

FLG nanosheets were synthesized from natural graphite flakes by using microwave irradiation. Graphite flakes were mixed with sodium tungstate and hydrogen peroxide in the ratio (1:0.1:4) and the mixture solution was sonicated for 1 hour. Then the mixture was refluxed in a high temperature microwave sintering furnace (2.45 GHz, 0-1.95 kW) at a power of 1200 W for 100 s. Under microwave irradiation, the precursors exfoliated rapidly, accompanied by sparks and violent fuming. After the microwave treatment, the suspension was ultrasonicated and centrifuged to remove the unreacted graphite. The supernatant was filtered and the solid obtained was washed repeatedly with distilled water and freeze dried for further use.

Characterization

The morphological analysis of FLG nanosheets was done by field emission scanning electron microscopy (FESEM) and transmission electron microscopy (TEM) using Zeiss Ultra 55 field emission scanning electron microscope and JEOL TEM-2100, respectively. X-ray diffraction (XRD) measurements were conducted using a D8 Advance (Bruker) X-ray diffractometer with Cu Kα radiation (λ=1.5418 Å). Brunauer-Emmett-Teller (BET) surface area analysis was done by recording nitrogen adsorption/desorption isotherms at 77 K on a Micromeritics ASAP 2020 apparatus. Prior to analysis, samples were degassed at 200 °C in vacuum for 24 h. The specific surface area (SSA) was calculated by the BET method based on adsorption data in the relative pressure (ρ/ρ^o) range of 0.05 to 0.3. The total pore volume was measured from the amount of nitrogen adsorbed at a relative pressure (ρ/ρ^o) of 0.99. The pore size distribution (PSD) was analyzed using a non-local density functional theory (NLDFT) method with a slit pore model from the nitrogen desorption data. X-ray photoelectron spectroscopy (XPS) data were taken on an AXIS Ultra instrument from Kratos Analytical in the range of 1-1300 eV to investigate the surface chemical composition of the obtained product. Raman spectra were collected using Seki Technotron STR 300 laser Raman spectrometer using laser excitation at 514.5 nm.

Fabrication of the supercapacitor

The supercapacitor electrodes have been fabricated as follows: As-synthesized FLG nanosheets and $EMIMBF_4$ (1:1 w/w) were dispersed in isopropanol by ultrasonication (SONICS Vibra Cell) with 5% nafion solution as a binder. The electrodes were prepared by coating graphene dispersion (~6.5 mg of active material/electrode) on 2 cm × 2 cm sized Toray Carbon Paper (Alfa Aesar) using layer-by-layer brush coating technique. Coated carbon paper was heated in vacuum oven at 80 °C for 6 h to reduce the effect of binder used. The supercapacitor setup consists of FLG-coated carbon paper as electrodes, polypropylene membrane (Celgard) as separator, $EMIMBF_4$ as electrolyte and the stainless steel sheets as current collectors. Separator rinsed with $EMIMBF_4$ was sandwiched between two electrodes. This assembly was further sandwiched between current collectors. All the electrode preparation steps were carried out under glovebox conditions of < 0.1 ppm of water and oxygen content.

Electrochemical measurements

Electrochemical performances of the supercapacitor cells were tested by cyclic voltammetry (CV), galvanostatic charge/discharge and electrochemical impedance spectroscopy (EIS) on a computer controlled VERSA STAT 3 (Princeton Applied Research) potentiostat/galvanostat. All of the experiments were carried out in a two-electrode system. The potential range for CV measurements and galvanostatic charge/discharge tests was 0-3.5 V. EIS tests were carried out in the frequency range of 100 kHz-1 mHz by impressing a small 10 mV amplitude of ac signal.

Results and discussion

Synthesis of FLG

Graphite flakes, sodium tungstate and 30% hydrogen peroxide were mixed in the ratio 1:0.1:4 in a quartz round bottom flask. The plausible mechanism for the synthesis of FLG is intercalation of oxygen containing groups in between graphene layers and exfoliation. Hydrogen peroxide in the presence of sodium tungstate and microwave radiation intercalates epoxy moieties along the basal plane of stacked graphitic structure as shown in Fig. 1.[21, 22] The numerous localized defects in the π-structure of graphite serve as seed points for the oxidation process. Here, sodium tungstate plays a dual role i.e., it aids in oxidation as well as generation of defects in the π-structure of graphite. The co-operative alignment of epoxy groups leads to lattice constraints and initiates C-C unzipping. Epoxy diffusion is the key step for growth of defects as well as oxidative

cutting of graphene resulting in smaller domain size.[23] Meanwhile, the extended π-system and structural imperfections in graphite results in localized heating on microwave irradiation due to Joule heating.[24] The free movement of delocalised π-electrons results in ionisation of the surrounding atmosphere and generates microplasmas.[25] This results in superheating which contributes to a local deoxygenation reaction of intercalated graphite. Once the incipient graphenic structure is large enough for efficient Joule heating, it will act as another molecular heater, accelerating the deoxygenation and exfoliation.[26] The self-accelerated process was reflected by an abrupt volume expansion and a rise in temperature. The intercalation and deoxygenation reactions proceed simultaneously. The yield of graphene is about 58 wt.% with respect to the initial graphite precursor which is almost 5 times higher than the previously reported yields by similar greener methods.[27]

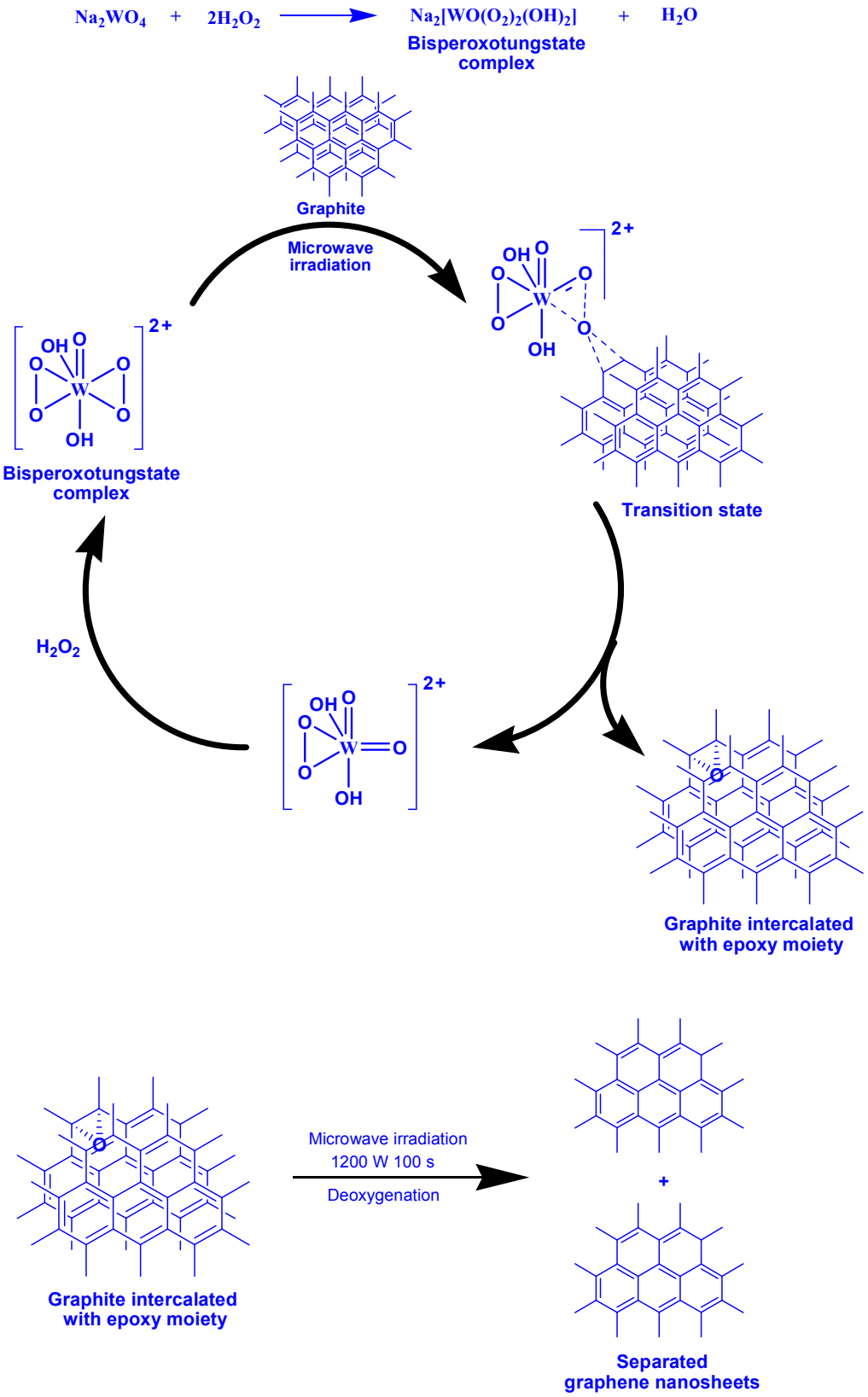

Fig. 1 Representative scheme of action of sodium tungstate on graphite and its regeneration.

The surface morphology of as-synthesized FLG was studied using FESEM and TEM. The low magnification FESEM image (Fig. 2a) clearly shows that the graphene sheets are uniformly exfoliated. The rapid deoxygenation reaction during exfoliation results in separation of graphitic layers which gives a fluffy morphology to the resulting graphene nanosheets. The high magnification FESEM (Fig. 2b) image shows thin and wrinkled platelets of graphene nanosheets that are transparent to the electron beam. Fig. 3a is a low magnification TEM image which shows many wrinkles and folded regions. The high magnification image (Fig. 3b) reveals thin transparent sheets folded at the edges which is a featured structure of graphene nanosheets.

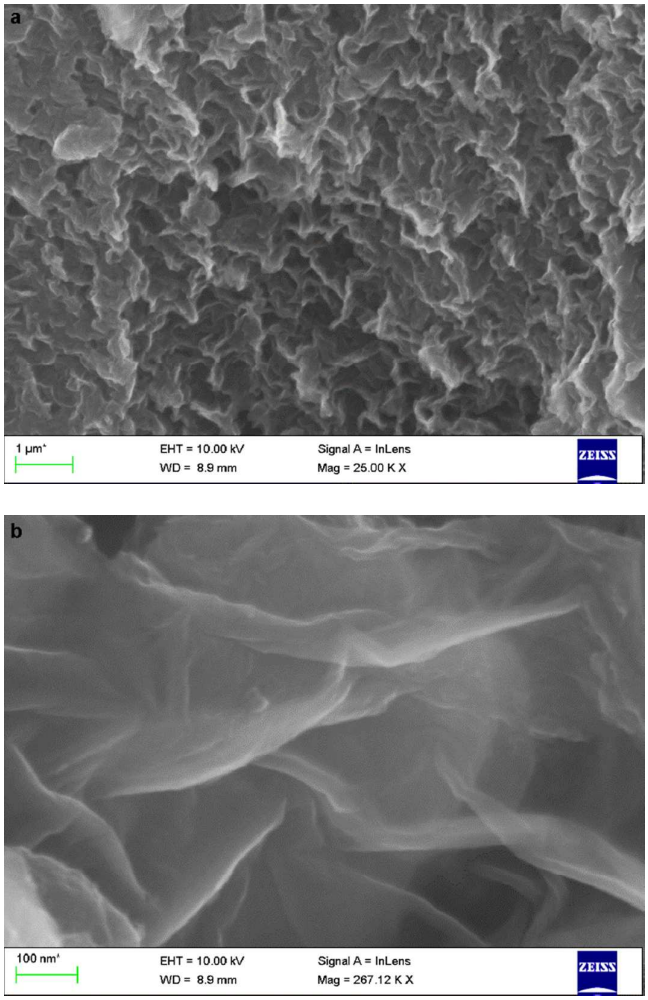

Fig. 2 FESEM image of graphene nanosheets (a) low magnification and (b) high magnification.

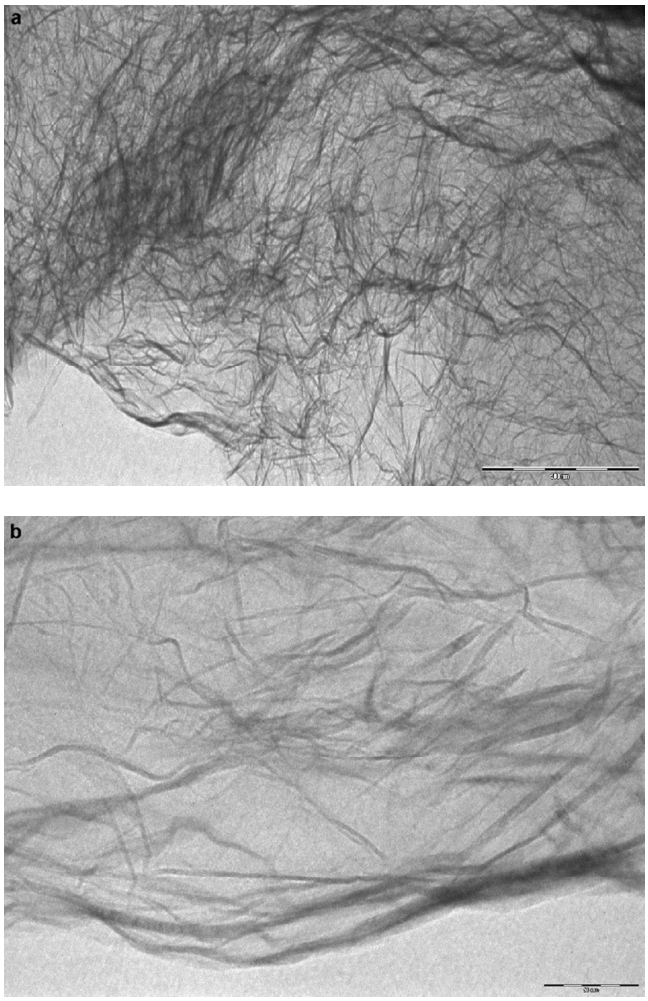

Fig. 3 TEM image of graphene nanosheets (a) low magnification and (b) high magnification.

A X-ray diffraction pattern of graphite and few layer graphene nanosheets has been displayed in Fig. 4. Graphite has an intense crystalline peak at ~26.5° corresponding to reflections from (002) plane. This sharp peak is due to the highly ordered stacking in graphite. In graphene this peak is replaced by a broad peak centered at $2\theta = 24.6°$, corresponding to the graphitic (002) profile with an interlayer spacing of 3.57 Å which is higher than that of graphite (3.33 Å). The broad nature of the peak can be attributed either to the small size of the layers or a relatively short domain order of the stacked sheets.[28] The average domain height (L_c) can be approximately determined to be 0.89 nm by using the Scherrer's equation[29] (ESI). It is known that the thickness of individual single layer graphene is 0.4 nm.[1] This suggests that most of the graphene should exist as bilayered nanosheets.

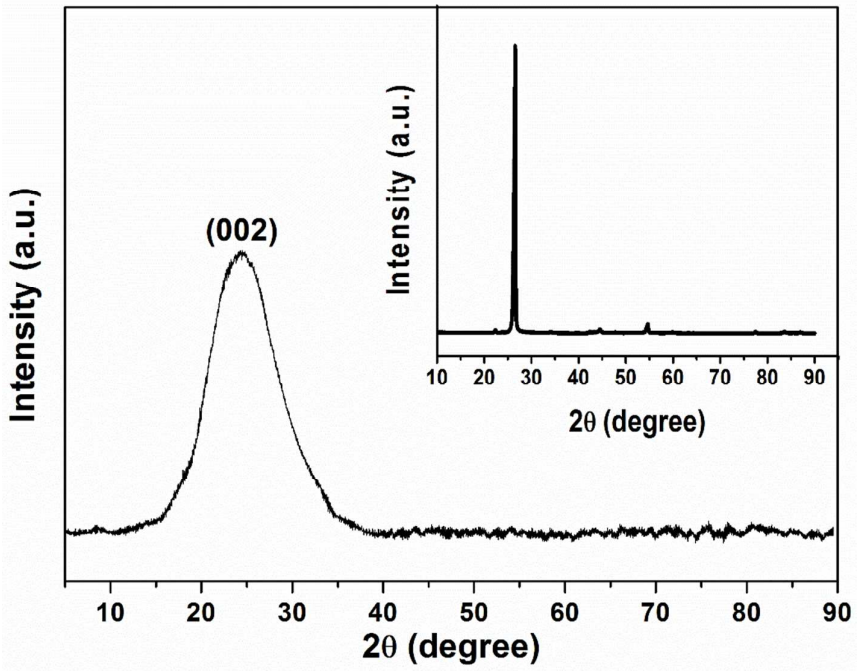

Fig. 4 XRD pattern of as-synthesized FLG nanosheets (inset shows the XRD pattern of graphite flakes).

The Raman spectrum of graphene provides valuable information regarding the presence of sp^2-sp^3 hybridization, the crystallite size, crystal disorder, defects, edge structure, number of graphene layers, etc.[30] The Raman spectrum of graphite (Fig. 5a) shows a sharp peak at 1581 cm^{-1}, corresponding to the two-fold degenerate E_{2g} mode at the zone centre. This peak is a characteristic of all sp^2 hybridized carbons and is called the G band. The disorder induced D band arising from the breathing mode of κ-point phonons of A_{1g} symmetry is related to the defects, i.e., edges and folds in graphene sheets.[31-33] The D-band is found at 1351 cm^{-1} with a very low intensity, suggesting that the graphite used is nearly defect free. The 2D band at 2729 cm^{-1} is attributed to the highest optical branch phonons near the κ-point at the Brillouin zone boundary.[34] The generation of defects by sodium tungstate was confirmed by running a control experiment wherin graphite flakes were treated with only sodium tungstate under microwave irradiation (1200 W for 100 s). The increase in intensity of D band confirms the generation of defects (Fig. 5a). Significant changes in the Raman spectra were observed on moving from graphite to graphene (Fig. 5b). Specifically, the G-band broadened significantly and displayed a blue-shift to 1589 cm^{-1} and the D band grew in intensity. The upshift in G-band indicates transformation of many layered graphite into few layered graphene nanosheets.[35] The increase in intensity of D band is due to the forced removal of oxygen at high temperature which creates strains and/or topological defects and results in smaller sp^2 domains.[36] The ratio of the G band to D band intensity (R) can be related to the in-plane crystallite size, L_a by equation (1).[37]

$$L_a(nm) = \frac{4.4}{R} \quad (1)$$

The as-calculated domain size of FLG nanosheets is 3.9 nm. Thus, the blue-shift of the G band and relatively intense D band indicate small stacks of quite disordered graphene sheets. The second-order Raman feature, namely the 2D band is red-shifted to 2710 cm^{-1}. The 2D band is very sensitive to the stacking order of the graphene sheets along the c-axis as well as to the number of layers. The number of layers of graphene sheets can be distinguished from the relative intensity ratio of I_{2D}/I_G, where I_{2D} and I_G are the relative intensities of 2D and G bands respectively. The intensity ratio I_{2D}/I_G of >2, 1-2, and <1 correspond to single-layered, double-layered and multi-layered graphene, respectively.[38] An I_{2D}/I_G intensity ratio of 1.1 verifies bilayered graphene nanosheets.

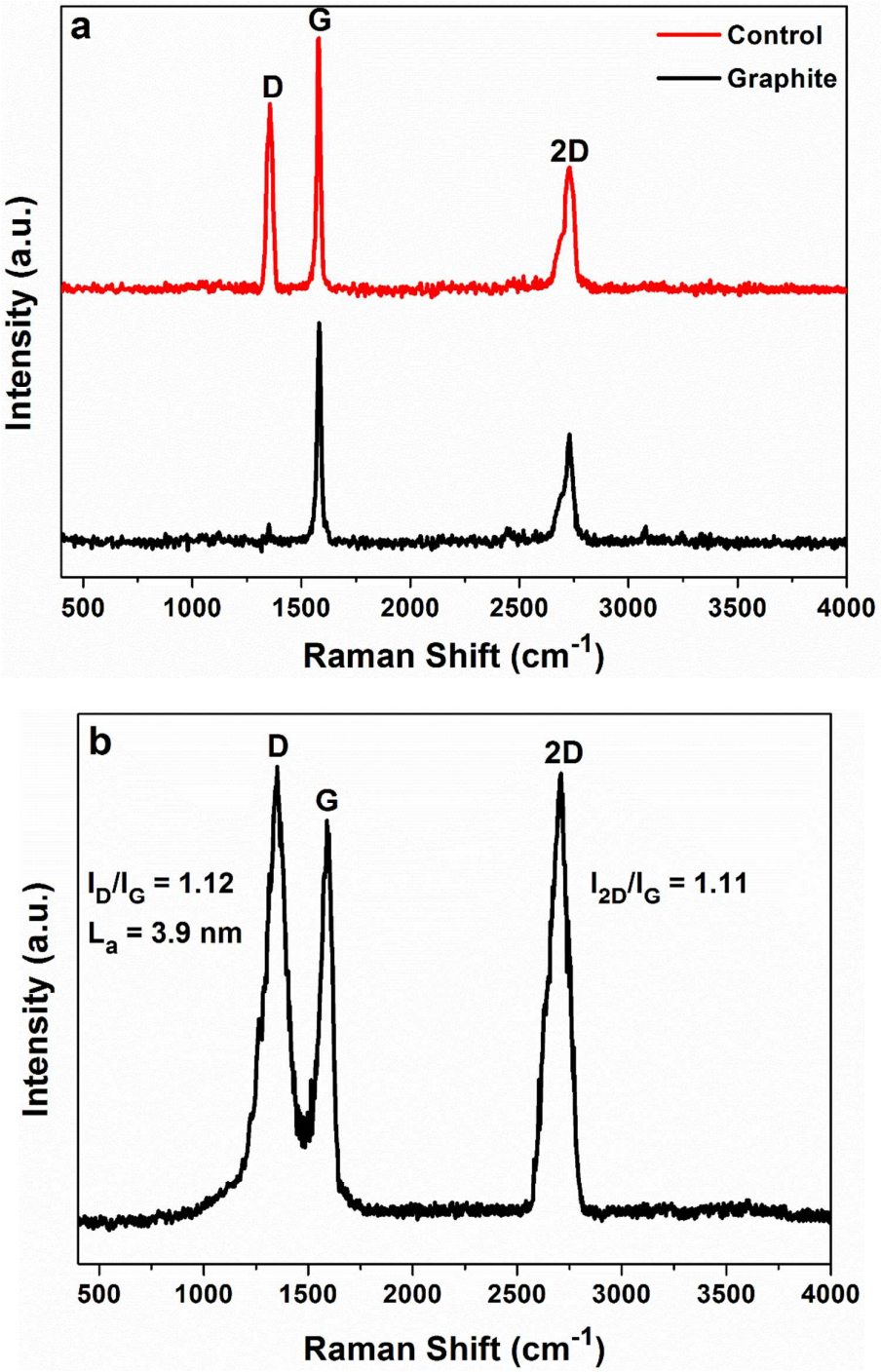

Fig. 5 Raman spectra of (a) graphite and control experiment; (b) FLG nanosheets.

The chemical composition of FLG nanosheets was analyzed by X-ray photoelectron spectroscopy (XPS). The wide survey XPS spectrum and its C1s, O1s peaks are shown in Fig. 6 (a), (b) and (c) respectively. It indicates FLG nanosheets mainly contain carbon (95.72 at.%) and oxygen (4.1 at.%). The low oxygen content indicates almost complete deoxygenation. High-resolution C1s spectrum shows well-defined sharp peak at 284.5 eV with an asymmetric tail towards higher binding energy. It indicates that the sample contains high concentration of sp^2 carbon.[39] The sharpness of C1s peak is indicative of low content of other functional groups.[40] The deconvolution of C1s spectrum reveal two main oxygen component peaks present in FLG nanosheets, C-O-C at 286 eV and carboxylate at 288.8 eV, respectively and a π-π^* satellite peak at 291.2 eV (assigned to π electrons delocalised at the aromatic network of graphene).[41] The deconvolution of O1s peak gives two peaks at 532 and 533.5 eV which are attributed to C=O and C-O, respectively.[42] Furthermore, FLG nanosheets has a high C/O

atomic ratio of ~9.6 almost four times higher than that reported for microwave assisted synthesis of graphene.[43] It is worthy to note that the at.% of carbon in FLG nanosheets is higher than the values reported for chemically and thermally reduced graphene oxide.[44, 45]

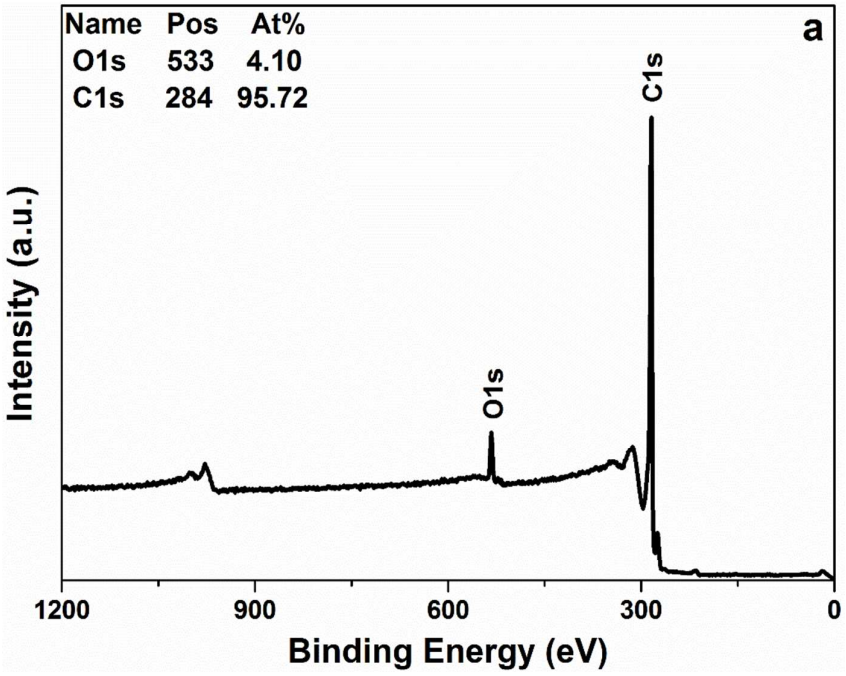

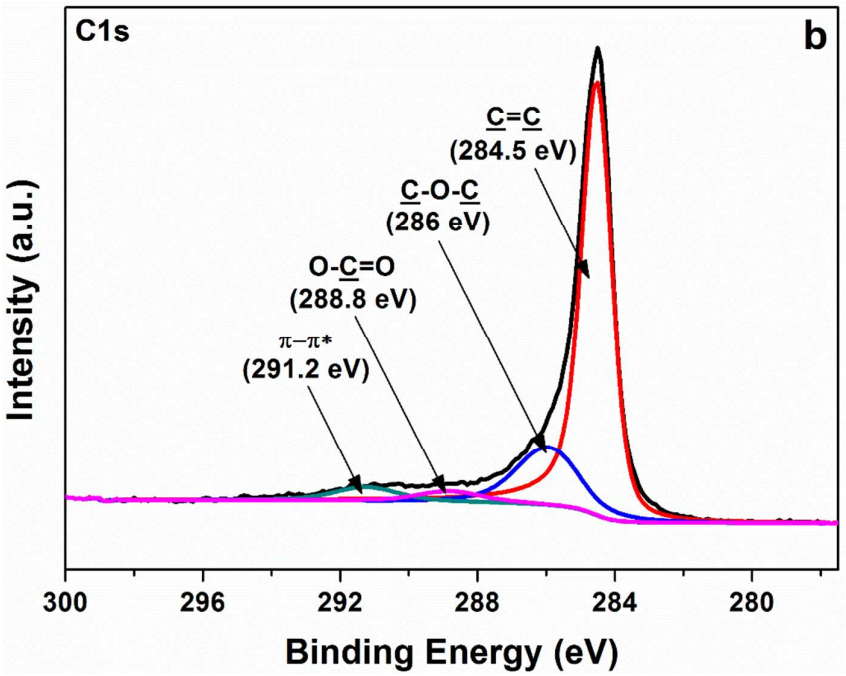

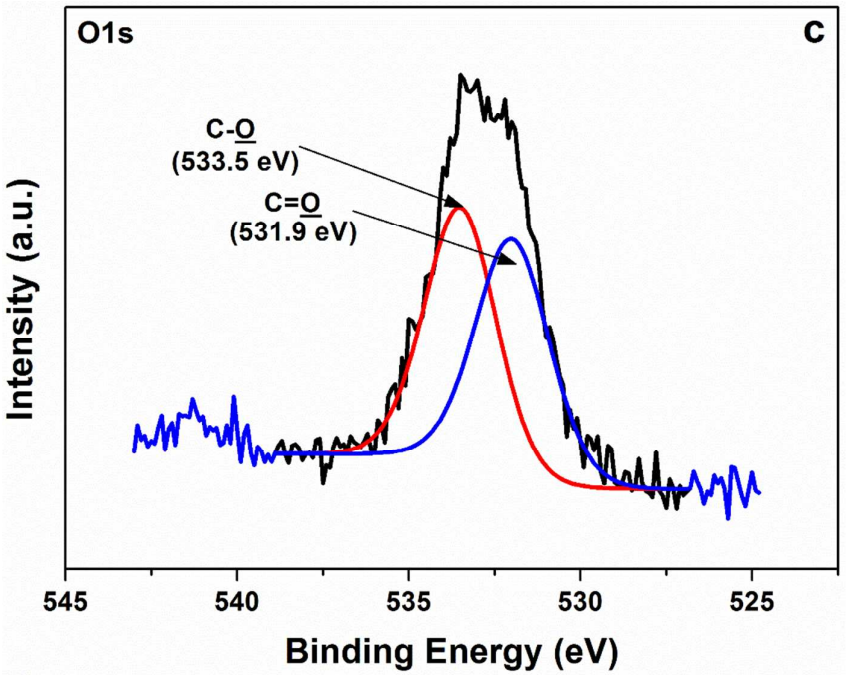

Fig. 6 XPS spectra of as-synthesized FLG nanosheets (a) wide scan spectrum; (b) C1s spectrum and (c) O1s spectrum

The surface area and porosity of as-synthesized FLG nanosheets was analysed by N_2 gas adsorption-desorption isotherms. The isotherm (Fig. 7a) exhibits a characteristic type-IV pattern with a pronounced hysteresis in the ρ/ρ^o range 0.4-1.0, implying the presence of a large number of mesopores in FLG nanosheets. . The specific surface area was estimated using the Brunauer-Emmett-Teller (BET) method which was found to be 1103.62 $m^2 g^{-1}$, roughly 3 times higher than the graphene prepared by exfoliation of GO in microwave irradiation.[43] The observed increase in surface area of FLG nanosheets compared to graphene synthesized by similar methods is due to the smaller graphene domains where significant contribution for the specific surface area comes from the edge part.[29] As evaluated by BET measurements, the surface area of FLG nanosheets arising from micro- and meso-pores were estimated to be 61.1% and 31.9% of the total measured area, respectively. The pore size distribution (PSD) plot (Fig. 7b) indicates bimodal pore size distribution i.e., micropores of 1.81 nm and mesopores of 3.9 nm. This type of porosity integrates both high capacitance (microporosity)[46] and fast kinetics (mesoporosity).[47, 48] High surface area and bimodal pore size distribution of FLG nanosheets are the highlights of our method of synthesis.

v

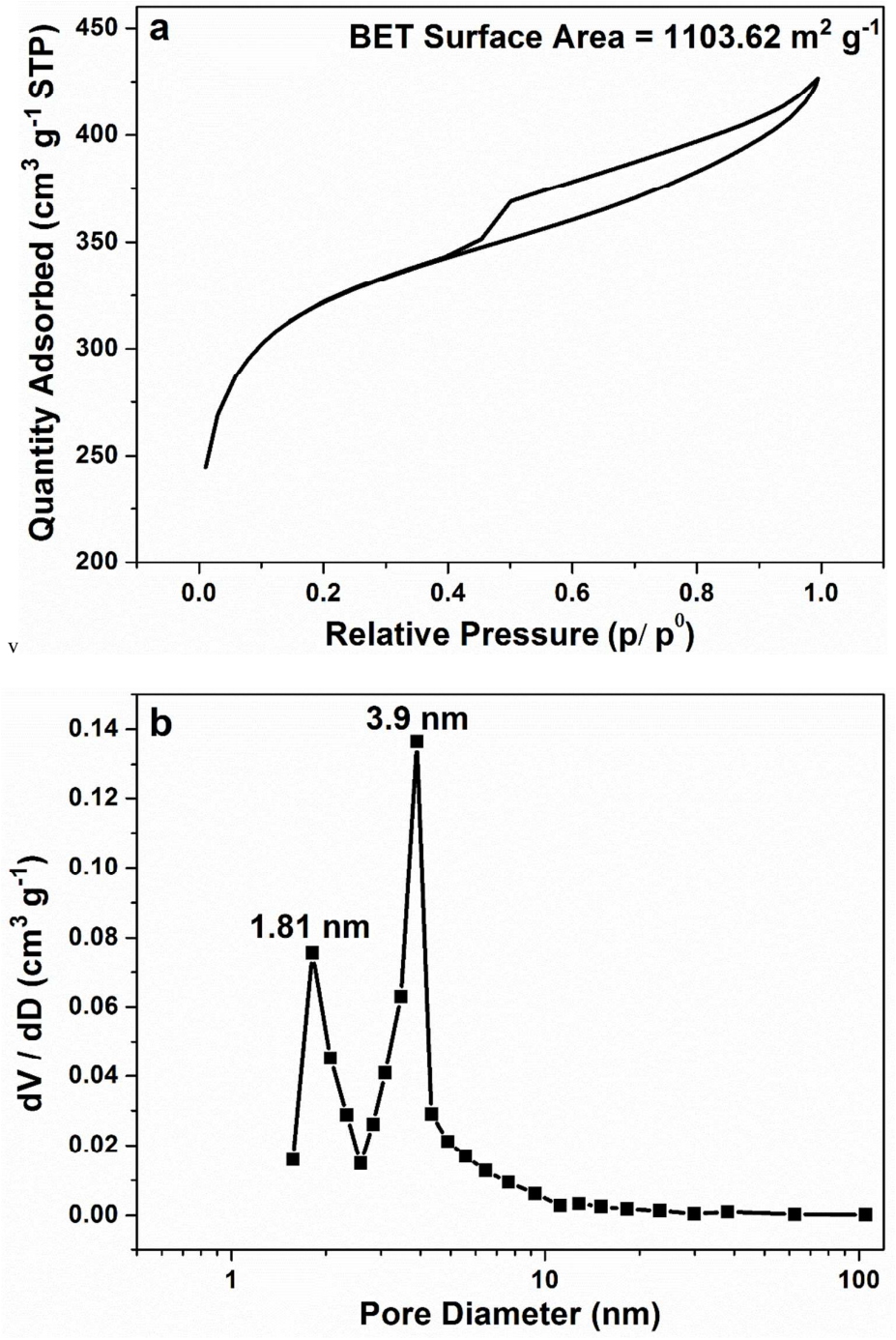

Fig. 7 (a) Nitrogen sorption isotherm of FLG nanosheets measured at 77 K and (b) PSD curves of FLG nanosheets calculated by BJH method

In addition to obtaining high quality graphene nanosheets through the proposed synthetic route sodium tungstate shows an excellent regeneration capability of 100% as demonstrated by at least 3 recycling experiments for more practical applications. The mechanism of regeneration of catalyst is as shown in Fig 1. The percentage yield of graphene remains unchanged at 62 wt.% from 1R to 3R. From Raman analysis (Fig. 8), it is confirmed that the I_D/I_G ratio and I_{2D}/I_G ratio is preserved for 1R indicating the domain size and the layer number of graphene nanosheets remains unchanged. However for 3R the I_D/I_G ratio changes to 1 indicating increase in domain size of graphene nanosheets whereas the layer number remains unchanged. Results are summarized in Table 1.

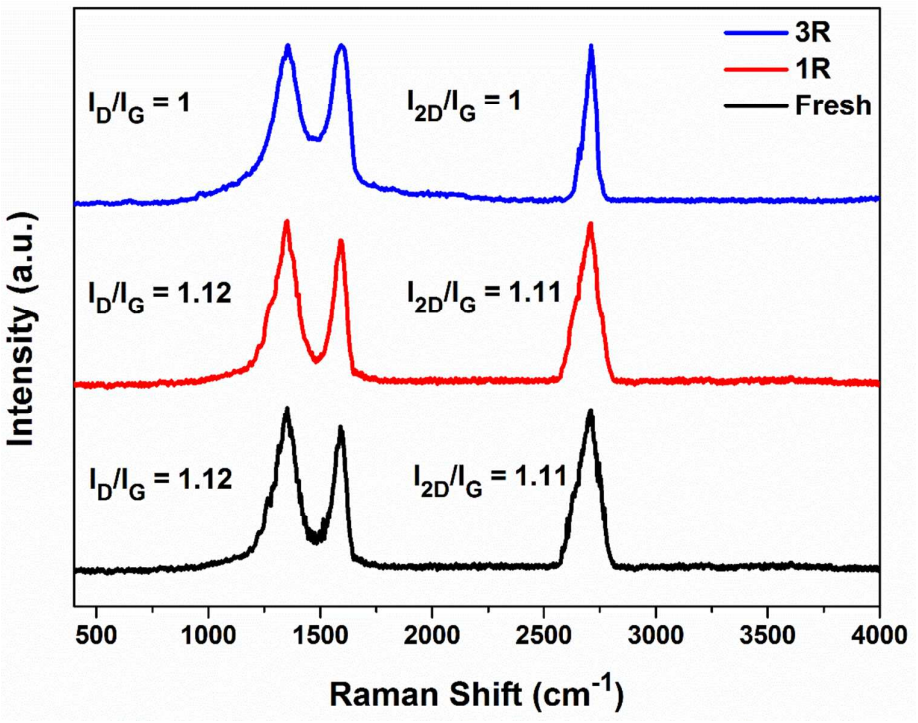

Fig. 8 Raman spectra of FLG nanosheets obtained from fresh and regenerated sodium tungstate catalyst

$Na_2WO_4.2H_2O$	% Yield	I_D/I_G	I_{2D}/I_G
Fresh	58 wt. %	1.12	1.11
1R	58 wt. %	1.12	1.11
3R	58 wt.%	1	1

Table 1 Percentage yield, I_D/I_G and I_{2D}/I_G ratios of FLG nanosheets obtained from fresh and regenerated sodium tungstate catalyst.

Electrochemical studies

The electrochemical analysis has been carried out using the best practice method, a two-electrode supercapacitor setup and performance is reported in terms of mass of the active electrode material. $EMIMBF_4$ with a wide electrochemical window of 3.5 V, was selected as the electrolyte for FLG based supercapacitors. CV is considered as an ideal method for characterizing the capacitive behaviour of any material. Fig. 9 shows the CV curves of FLG electrodes at a scan rate of 10-100 mV s^{-1} in the potential range of 0-3.5 V using neat $EMIMBF_4$ electrolyte. It can be seen that the CV curve of FLG electrodes at a low scan rate of 10 mV s^{-1} exhibit a sharp rectangular shape with no pseudocapacitive peaks visible, indicating the capacitive response of FLG nanosheets stems from only electrical double-layer formation and not electrochemical oxidation/reduction.[49, 50] Even at higher scan rates of upto 100 mV s^{-1} the CV curves maintain a rectangular shape indicating excellent rate capability and low ionic resistance.[51] The tiny amount of oxygen functionalised groups present on the surface of FLG nanosheets have no pseudocapacitive contribution because in the case of ionic liquid (IL) electrolyte the presence of oxygen surface groups has no significant effect on the performance of FLG nanosheets because protons are not available.[52] The gravimetric specific capacitance, C_s (F g^{-1}), was calculated according to equation (2)[53]

$$C_s = \frac{4I}{m\frac{dV}{dt}} \quad (2)$$

where I is the average current (A) during discharge (from V_{max} to zero volts), m is the total mass of the active material in two electrodes (g) and dV/dt (V s^{-1}) is the scan rate. A highest capacitance value of 212 F g^{-1} was obtained at a scan rate of 10 mV s^{-1}.

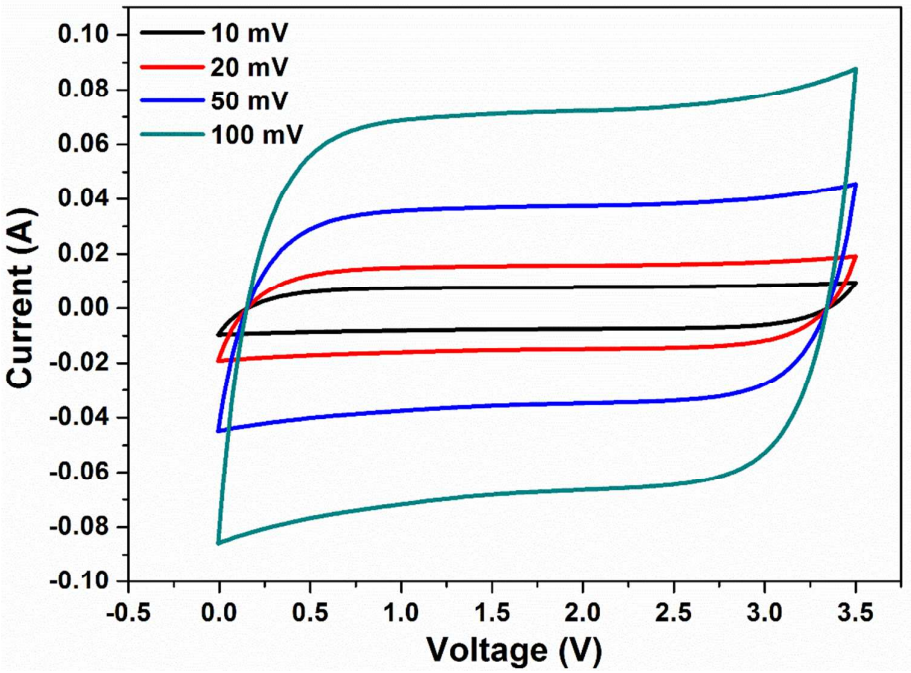

Fig. 9 Cyclic voltammograms of FLG based supercapacitor at scan rates of 10-100 mV s^{-1} in the range of 0-3.5 V

To further evaluate the electrochemical properties galvanostatic charging and discharging of the FLG electrodes in neat $EMIMBF_4$ electrolyte was performed. The charge-discharge curves (Fig. 10a) display linear response at different current densities (1-10 A g^{-1}) between 0.0 and 3.5 V and are symmetrical that are very typical of pure double-layer capacitors. Even at a high current density of 10 A g^{-1}, the charge-discharge curve still possess good symmetry revealing that the FLG electrode shows excellent electrochemical reversibility.[54, 55] The gravimetric specific capacitance, C_s (F g^{-1}), was calculated according to equation (3)[53]

$$C_s = \frac{4I}{m\frac{dV}{dt}} \quad (3)$$

where I is the constant current (A), m is the total mass of two electrodes (g) and dV/dt (V s^{-1}) is the slope obtained by fitting a straight line to the discharge curve over the range of V (the voltage at the beginning of discharge after correcting for iR drop) to ½ V. A maximum capacitance of 219 F g^{-1} was obtained for applied current density of 1 A g^{-1}. The specific capacitance of as-synthesized FLG based electrodes is higher than most of the values reported so far in two electrode configuration in IL electrolyte.[56, 57] Furthermore, as the current density increases the capacitance decreases indicating the strong dependence of the specific capacitance on the current density (Fig 10b). This is because at high current density diffusion of electrolyte ions is limited and hence interior surface of the electrode are inaccessible due to concentration polarization phenomenon.[58, 59] Even under a high current density of 10 A g^{-1}, nearly 86.75% of the initial capacitance is maintained for FLG electrodes in $EMIMBF_4$ electrolyte. These results indicate that FLG electrodes allow rapid ion diffusion and have extremely good rate capability.

The higher electrochemical properties of FLG electrodes can be explained by PSD and effective-specific surface area (E-SSA). For IL electrolyte systems the ion-accessible surface area is strongly influenced by the relative sizes of the pores and the IL ions. FLG nanosheets has a bimodal pore size distribution (micropores of 1.81 nm and mesopores of 3.99 nm) and IL ion $EMIM^+$ has a diameter of 0.75 nm. As the pore size in FLG nanosheets is higher than the ion size of the electrolyte ions easy accessibility of the electrode surface by electrolyte ions is possible. This results in increased ion-accessible surface area which in turn improves the charge storage. Also the mesoporous channels facilitate rapid ion transport at high scan rates thereby decreasing the resistance for charge diffusion.

Cycle life is one of the most important requirements in practical applications of supercapacitor. Fig. 10 (c) shows the cyclic stability of FLG electrodes at a constant current density of 5 A g^{-1} for 3000 cycles. More than 95% of its initial capacitance is retained even after 3000 cycles which indicates both good high-rate performance and excellent stability of FLG electrodes. There is no significant difference in iR drop after long cycles which also indicates the good stability of the electrode. In order to evaluate the device performance of FLG based supercapacitor, the energy density (E) and power density (P) calculated from galvanostatic discharge curves are plotted on the Ragone plot (Fig. 10d). The energy density E (W h kg^{-1}) and power density P (kW kg^{-1}) were calculated according to equations (4)[60] and (5)[61] respectively.

$$E = \frac{1000 \times C_s \times V^2}{4 \times 2 \times 3600} \quad (4)$$

where C_s is the specific capacitance of the cell, V is the cell voltage after correcting for iR drop.

$$P = \frac{E}{t_d} \quad (5)$$

where t_d is the discharging time.

FLG electrodes show maximum performance with a highest energy density of 83.56 W h kg^{-1} at a power density of 1.66 kW kg^{-1} at 1 A g^{-1} which gradually reduces to 61.57 W h kg^{-1} at 15.3 kW kg^{-1} at a current density of 10 A g^{-1} as depicted in the Ragone plot (Fig. 10d). The wettability of FLG electrodes and large electrochemical voltage window of $EMIMBF_4$ are the vital factors which contribute to high the energy density. When compared with other graphene based electrodes reported in the literature, in $EMIMBF_4$ electrolyte, FLG based electrodes possess comparable energy density with superior power capability.[56] This implies that we have a supercapacitor capable of storing 72.67 W h kg^{-1} (equivalent to that of Ni metal hydride battery) and can be recharged in less than 40 seconds.[62]

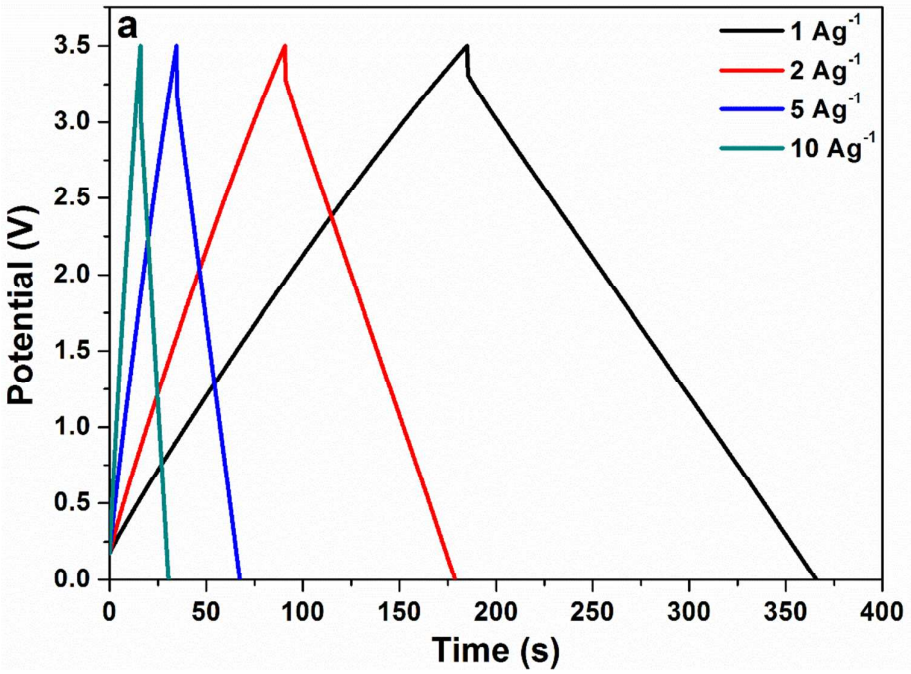

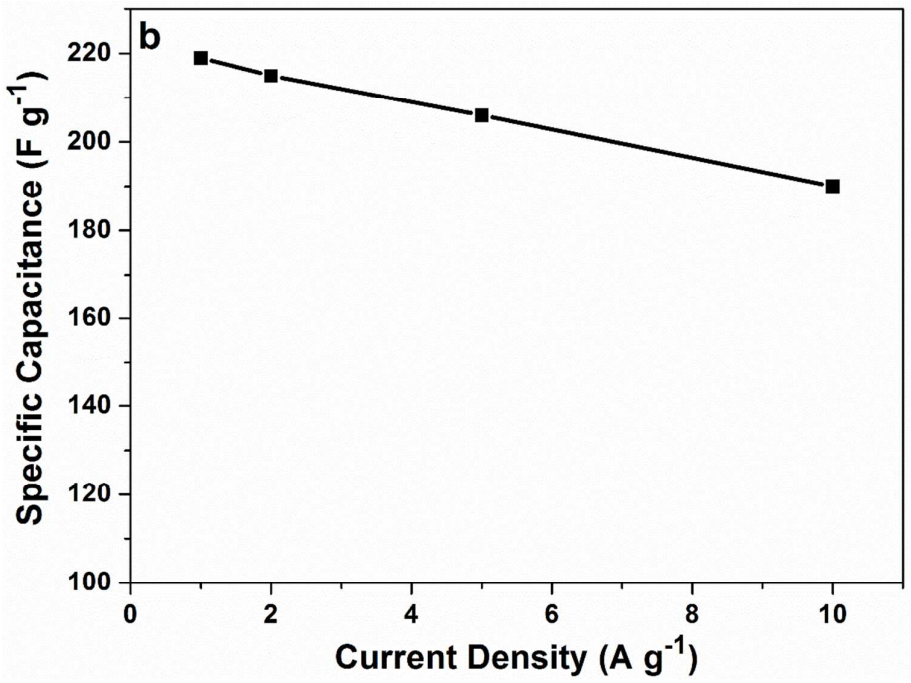
b
Specific Capacitance (F g-1)
220
200
180
160
140
120
100
0
2
4
6
8
10
Current Density (A g-1)

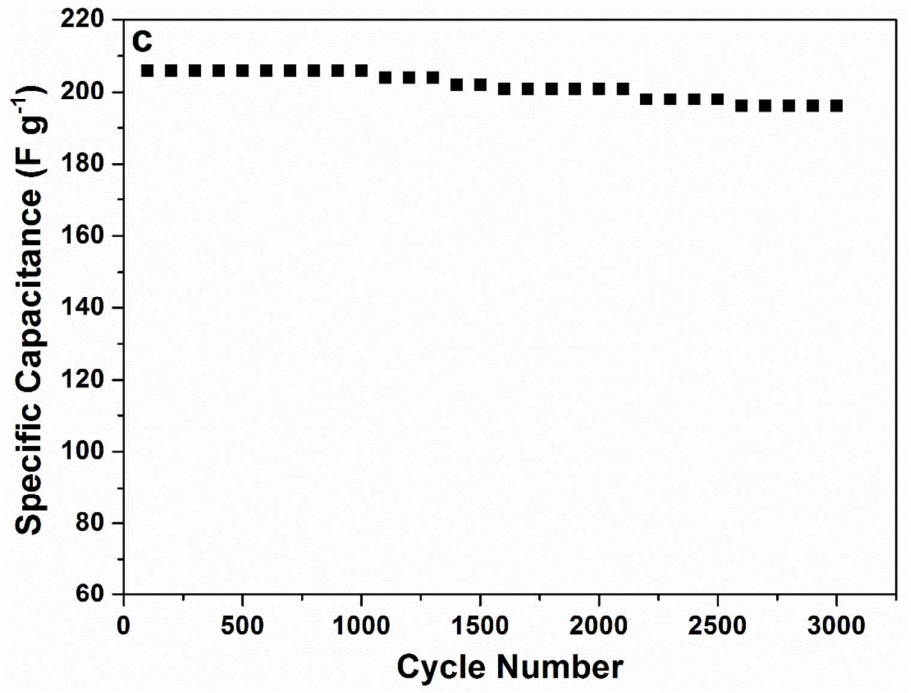
c
Specific Capacitance (F g-1)
220
200
180
160
140
120
100
80
60
0
500
1000
1500
2000
2500
3000
Cycle Number

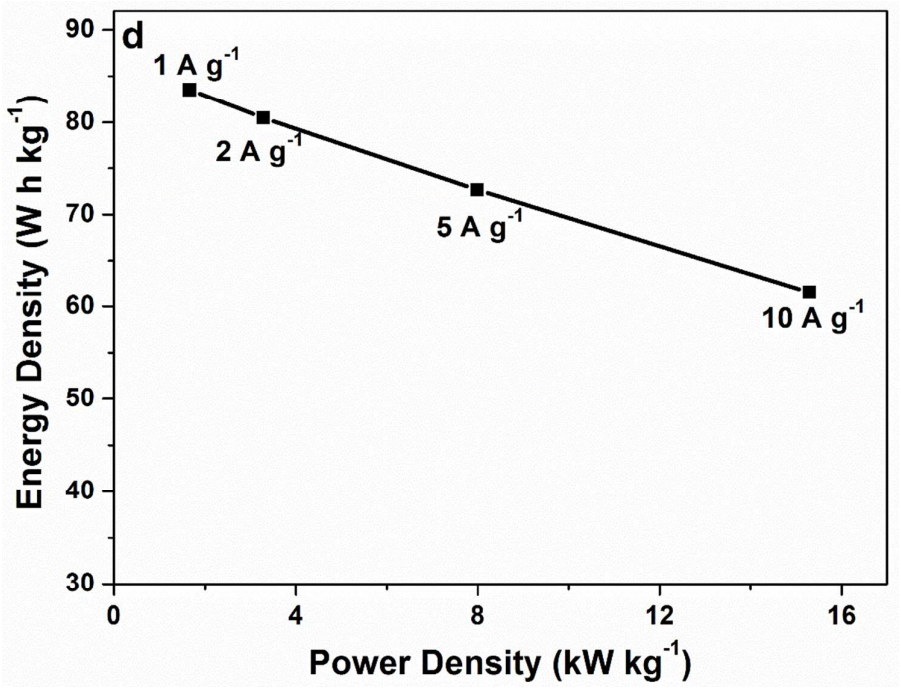

Fig. 10 (a) Galvanostatic charge-discharge curves of FLG nanosheets at constant current densities of 1-10 A g^{-1} in neat $EMIMBF_4$ electrolyte; (b) Specific-capacitance change as a function of current density; (c) Specific capacitance change at a constant current density of 5 A g^{-1} as a function of cycle number and (d) Ragone plot relating energy density to power density of FLG based electrode in neat $EMIMBF_4$ electrolyte.

As an attempt to understand the fundamental behaviour of electrode materials for supercapacitors EIS analysis was also performed. EIS of FLG electrodes in $EMIMBF_4$ electrolyte has been measured in the frequency range from 100 kHz-1 mHz at an open circuit potential with an ac amplitude of 10 mV. Shown in Fig. 11 is the Nyquist plot of FLG electrodes in neat $EMIMBF_4$ electrolyte. The intersection of the curves at the X-axis in the high frequency region corresponds to the equivalent series resistance (ESR) of the electrodes. The ESR of FLG material is 0.13 Ω which signifies the high conductivity of as-synthesized FLG nanosheets. The low ESR is responsible for the high power capability of FLG electrodes.[63] Charge transfer resistance within the FLG nanosheets is low which is evident from the smaller diameter semicircle (0.2 Ω) indicating higher diffusion rate of ions into the pores.[64] The steep Warburg region indicates fast ion transport through the pores and efficient access of electrolyte ions to the electrode surface.[65] The nearly vertical line in the low frequency region indicates pure double layer capacitive behaviour.[7] In a typical double layer capacitor the 'knee' frequency, i.e., the transition point from Warburg region to low frequency region, corresponds to the double layer charge saturation. The Nyquist plot reveals the 'knee' frequency is located at around 72.57 Hz suggesting that most of its stored energy is accessible at frequencies as high as 72.57 Hz. Moreover, higher knee frequency indicates easier accessibility of electrolyte ions into pores and hence a better rate performance of FLG electrodes.[66] These observations are consistent with the results obtained from cyclic voltammetry and charge discharge studies. The obtained impedance spectra was also analysed by an equivalent circuit (inset in Fig. 12) consisting series and parallel combinations of equivalent series resistance (R_s), electrical double layer capacitance (C_{dl}), charge transfer resistance (R_{ct}), Warburg diffusion element (W), leakage resistance (R_{leak}) and mass capacitance (C_l) using ZsimpWin 3.21 commercial software.[67] As shown in Fig. 12, the fitting curves coincide well with their corresponding curves, implying that the equivalent circuit model reasonably reflects the electrochemical processes occurring on/within the graphene nanosheets. The mean error of modulus is less than 5%, indicating that these fitting values are highly accurate. The slight offset in the simulated Nyquist plot as compared to the originally measured Nyquist plot of FLG electrodes in the low frequency range can be explained as follows: The diffusion resistance is responsible for the Nyquist plot to be inclined to the -Z" axis in the low frequency region. Since the FLG based supercapacitor has very low diffusion resistance due to an ideal pore size distribution the low frequency region shows an almost ideal capacitive behaviour more than that expected from simulation results. The ideal pore size distribution is also responsible for the high penetrability of ac signal inside the FLG electrode and hence there is lesser frequency dispersion than expected from the simulated electrode.

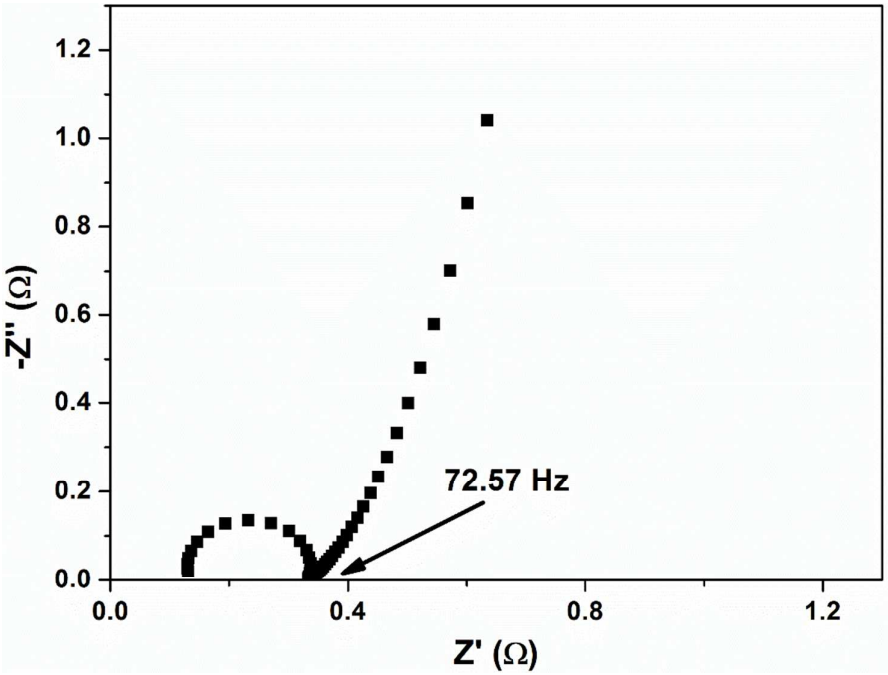

Fig. 11 Nyquist plot of FLG based supercapacitor in $EMIMBF_4$ electrolyte. (Amplitude: 10 mV; Range 100 kHz –1 mHz)

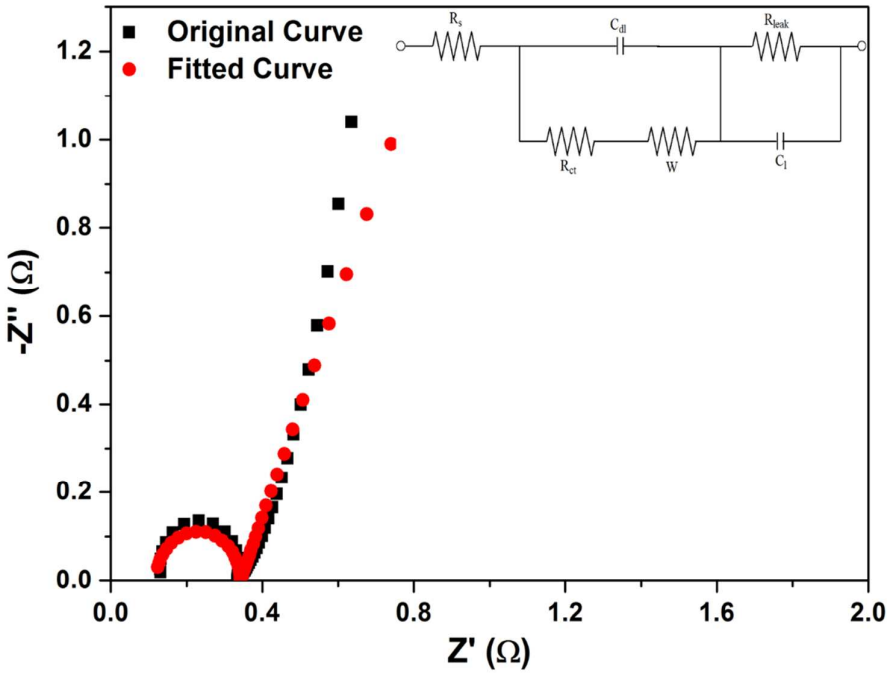

Fig. 12 Equivalent circuit simulation results from the Nyquist plot of FLG electrodes (inset shows the equivalent circuit used to simulate the FLG based supercapacitor).

Conclusion

In conclusion, we report a microwave assisted green method for the synthesis of high quality graphene nanosheets directly from graphite flakes in aqueous medium using a regenerative catalyst, sodium tungstate. The method is highly efficient, producing more than 50% yield, which is approximately 5 times more than the previously reported yields.[27] Raman spectroscopy analysis reveals that the graphene nanosheets are bilayered, with a domain size of 3.9 nm which is responsible for the large specific surface area (S_{BET} = 1103.62 m^2 g^{-1}). X-ray photoelectron spectroscopy analysis indicates that the as-synthesized graphene has negligible oxygen functionality (4.1 at.%) and a high C/O ratio (~9.6). The as-synthesized graphene nanosheets showed excellent electrochemical performance in terms of high capacitance (219 F g^{-1}), high energy density (83.56 W h kg^{-1}) and power density (15.29 kW kg^{-1}) as well as an excellent cyclability (3000 cycles). This can be attributed to the high conductivity and effective usage of the entire electrode surface area by electrolyte ions due to an ideal pore size distribution. They show a high frequency capacitive response with a knee frequency of 72.57 Hz which can be accounted for by the large and accessible surface area of graphene nanosheets. Hence, this green approach is a viable low-cost route for the large scale synthesis of high quality graphene nanosheets directly from graphite for supercapacitor applications.

Acknowledgments

The authors would like to thank Indian Institute of Technology-Bombay and Centre for Nanoscience and Engineering-IISc, Bangalore for providing necessary characterization facilities. The authors are grateful to National Institute of Technology Karnataka-Surathkal, for providing financial assistance in the form of Institute fellowship along with necessary facilities and infrastructure to carry out the present work. Special thanks to Dr. David J Morgan, Postdoctoral Research Associate, Cardiff Catalysis Institute, School of Chemistry, Cardiff University for extending help in the interpretation of XPS results.

Notes and reference

† Electronic Supplementary Information (ESI) available: [Energy Dispersive X-ray spectrum of graphene nanosheets and Scherrer equation]. See DOI: 10.1039/c000000x/

1. A. K. Geim and K. S. Novoselov, *Nat. Mater.*, 2007, 6, 183-191.
2. K. S. Novoselov, A. K. Geim, S. Morozov, D. Jiang, Y. Zhang, S. Dubonos, I. Grigorieva and A. Firsov, *Science*, 2004, 306, 666-669.
3. J. C. Meyer, A. K. Geim, M. I. Katsnelson, K. S. Novoselov, T. J. Booth and S. Roth, *Nature*, 2007, 446, 60-63.
4. S. V. Morozov, K. S. Novoselov, M. I. Katsnelson, F. Schedin, D. C. Elias, J. A. Jaszczak and A. K. Geim, *Phys. Rev. Lett.*, 2008, 100, 016602.
5. C. Lee, X. Wei, J. W. Kysar and J. Hone, *Science*, 2008, 321, 385-388.
6. Y. Zhu, S. Murali, W. Cai, X. Li, J. W. Suk, J. R. Potts and R. S. Ruoff, *Adv. Mater.*, 2010, 22, 3906-3924.
7. M. D. Stoller, S. Park, Y. Zhu, J. An and R. S. Ruoff, *Nano Lett.*, 2008, 8, 3498-3502.
8. S. Vivekchand, C. S. Rout, K. Subrahmanyam, A. Govindaraj and C. Rao, *J. Chem. Sci. (Bangalore, India)*, 2008, 120, 9-13.
9. C. Berger, Z. Song, T. Li, X. Li, A. Y. Ogbazghi, R. Feng, Z. Dai, A. N. Marchenkov, E. H. Conrad, P. N. First and W. A. de Heer, *J. Phys. Chem. B*, 2004, 108, 19912-19916.
10. P. W. Sutter, J.-I. Flege and E. A. Sutter, *Nat. Mater.*, 2008, 7, 406-411.
11. X. Li, C. W. Magnuson, A. Venugopal, J. An, J. W. Suk, B. Han, M. Borysiak, W. Cai, A. Velamakanni, Y. Zhu, L. Fu, E. M. Vogel, E. Voelkl, L. Colombo and R. S. Ruoff, *Nano Lett.*, 2010, 10, 4328-4334.
12. X. Li, X. Wang, L. Zhang, S. Lee and H. Dai, *Science*, 2008, 319, 1229-1232.
13. Y. Hernandez, V. Nicolosi, M. Lotya, F. M. Blighe, Z. Sun, S. De, I. McGovern, B. Holland, M. Byrne and Y. K. Gun'Ko, *Nat. Nanotechnol.*, 2008, 3, 563-568.
14. A. B. Bourlinos, V. Georgakilas, R. Zboril, T. A. Steriotis and A. K. Stubos, *Small*, 2009, 5, 1841-1845.
15. D. Rangappa, K. Sone, M. Wang, U. K. Gautam, D. Golberg, H. Itoh, M. Ichihara and I. Honma, *Chemistry – A European Journal*, 2010, 16, 6488-6494.
16. S. Stankovich, D. A. Dikin, R. D. Piner, K. A. Kohlhaas, A. Kleinhammes, Y. Jia, Y. Wu, S. T. Nguyen and R. S. Ruoff, *Carbon*, 2007, 45, 1558-1565.
17. Y. Si and E. T. Samulski, *Nano Lett.*, 2008, 8, 1679-1682.
18. G. Wang, J. Yang, J. Park, X. Gou, B. Wang, H. Liu and J. Yao, *J. Phys. Chem. C*, 2008, 112, 8192-8195.
19. J. Liu, C. K. Poh, D. Zhan, L. Lai, S. H. Lim, L. Wang, X. Liu, N. Gopal Sahoo, C. Li, Z. Shen and J. Lin, *Nano Energy*, 2013, 2, 377-386.
20. J. Liu, H. Yang, S. G. Zhen, C. K. Poh, A. Chaurasia, J. Luo, X. Wu, E. K. L. Yeow, N. G. Sahoo, J. Lin and Z. Shen, *RSC Advances*, 2013, 3, 11745-11750.
21. R. Noyori, M. Aoki and K. Sato, *Chem. Commun.*, 2003, 1977-1986.
22. X. Liu, J. Liu, D. Zhan, J. Yan, J. Wang, D. Chao, L. Lai, M. Chen, J. Yin and Z. Shen, *RSC Advances*, 2013, 3, 11601-11606.
23. T. Sun and S. Fabris, *Nano Lett.*, 2011, 12, 17-21.
24. E. Vázquez and M. Prato, *ACS Nano*, 2009, 3, 3819-3824.
25. J. Menéndez, A. Arenillas, B. Fidalgo, Y. Fernández, L. Zubizarreta, E. Calvo and J. Bermúdez, *Fuel Process. Technol.*, 2010, 91, 1-8.
26. H. Hu, Z. Zhao, Q. Zhou, Y. Gogotsi and J. Qiu, *Carbon*, 2012, 50, 3267-3273.
27. G. S. Bang, H.-M. So, M. J. Lee and C. W. Ahn, *J. Mater. Chem.*, 2012, 22, 4806-4810.
28. V. Eswaraiah, S. S. Jyothirmayee Aravind and S. Ramaprabhu, *J. Mater. Chem.*, 2011, 21, 6800.
29. L. Zhang, F. Zhang, X. Yang, G. Long, Y. Wu, T. Zhang, K. Leng, Y. Huang, Y. Ma, A. Yu and Y. Chen, *Sci Rep*, 2013, 3, 1408.
30. M. S. Dresselhaus, A. Jorio, M. Hofmann, G. Dresselhaus and R. Saito, *Nano Lett.*, 2010, 10, 751-758.
31. F. Tuinstra, *The Journal of Chemical Physics*, 1970, 53, 1126.
32. A. Ferrari and J. Robertson, *Physical review B*, 2000, 61, 14095.
33. K. N. Kudin, B. Ozbas, H. C. Schniepp, R. K. Prud'Homme, I. A. Aksay and R. Car, *Nano Lett.*, 2008, 8, 36-41.

34. A. C. Ferrari, J. C. Meyer, V. Scardaci, C. Casiraghi, M. Lazzeri, F. Mauri, S. Piscanec, D. Jiang, K. S. Novoselov, S. Roth and A. K. Geim, *Phys. Rev. Lett.*, 2006, 97.
35. A. Gupta, G. Chen, P. Joshi, S. Tadigadapa and P. Eklund, *Nano Lett.*, 2006, 6, 2667-2673.
36. A. Ganguly, S. Sharma, P. Papakonstantinou and J. Hamilton, *J. Phys. Chem. C*, 2011, 115, 17009-17019.
37. D. S. Knight and W. B. White, *J. Mater. Res.*, 1989, 4, 385-393.
38. C. Shan, H. Tang, T. Wong, L. He and S. T. Lee, *Adv. Mater.*, 2012, 24, 2491-2495.
39. H. Ago, T. Kugler, F. Cacialli, W. R. Salaneck, M. S. Shaffer, A. H. Windle and R. H. Friend, *J. Phys. Chem. B*, 1999, 103, 8116-8121.
40. X. Wang, H. You, F. Liu, M. Li, L. Wan, S. Li, Q. Li, Y. Xu, R. Tian and Z. Yu, *Chem. Vap. Deposition*, 2009, 15, 53-56.
41. M.-C. Hsiao, S.-H. Liao, M.-Y. Yen, C.-C. Teng, S.-H. Lee, N.-W. Pu, C.-A. Wang, Y. Sung, M.-D. Ger, C.-C. M. Ma and M.-H. Hsiao, *J. Mater. Chem.*, 2010, 20, 8496-8505.
42. Y. Wen, H. Ding and Y. Shan, *Nanoscale*, 2011, 3, 4411-4417.
43. Y. Zhu, S. Murali, M. D. Stoller, A. Velamakanni, R. D. Piner and R. S. Ruoff, *Carbon*, 2010, 48, 2118-2122.
44. H. A. Becerril, J. Mao, Z. Liu, R. M. Stoltenberg, Z. Bao and Y. Chen, *ACS Nano*, 2008, 2, 463-470.
45. X. Dong, C.-Y. Su, W. Zhang, J. Zhao, Q. Ling, W. Huang, P. Chen and L.-J. Li, *PCCP*, 2010, 12, 2164-2169.
46. H. Yamada, H. Nakamura, F. Nakahara, I. Moriguchi and T. Kudo, *J. Phys. Chem. C*, 2007, 111, 227-233.
47. G.-J. Lee and S.-I. Pyun, *Langmuir*, 2006, 22, 10659-10665.
48. D.-W. Wang, F. Li, H.-T. Fang, M. Liu, G.-Q. Lu and H.-M. Cheng, *J. Phys. Chem. B*, 2006, 110, 8570-8575.
49. J. Yan, T. Wei, B. Shao, Z. Fan, W. Qian, M. Zhang and F. Wei, *Carbon*, 2010, 48, 487-493.
50. X. Wen, D. Zhang, L. Shi, T. Yan, H. Wang and J. Zhang, *J. Mater. Chem.*, 2012, 22, 23835-23844.
51. B.-J. Yoon, S.-H. Jeong, K.-H. Lee, H. Seok Kim, C. Gyung Park and J. Hun Han, *Chem. Phys. Lett.*, 2004, 388, 170-174.
52. R. Kötz and M. Carlen, *Electrochim. Acta*, 2000, 45, 2483-2498.
53. M. D. Stoller and R. S. Ruoff, *Energy & Environmental Science*, 2010, 3, 1294.
54. W.-w. Liu, X.-b. Yan, J.-w. Lang, J.-b. Pu and Q.-j. Xue, *New J. Chem.*, 2013, 37, 2186.
55. F. Zeng, Y. Kuang, G. Liu, R. Liu, Z. Huang, C. Fu and H. Zhou, *Nanoscale*, 2012, 4, 3997-4001.
56. C. Liu, Z. Yu, D. Neff, A. Zhamu and B. Z. Jang, *Nano Lett.*, 2010, DOI: 10.1021/nl102661q.
57. W.-Y. Tsai, R. Lin, S. Murali, L. Li Zhang, J. K. McDonough, R. S. Ruoff, P.-L. Taberna, Y. Gogotsi and P. Simon, *Nano Energy*, 2013, 2, 403-411.
58. D. W. Wang, F. Li, M. Liu, G. Q. Lu and H. M. Cheng, *Angew. Chem. Int. Ed.*, 2008, 47, 373-376.
59. C. Xu, J. Sun and L. Gao, *J. Mater. Chem.*, 2011, 21, 11253-11258.
60. Z. Bo, Z. Wen, H. Kim, G. Lu, K. Yu and J. Chen, *Carbon*, 2012, 50, 4379-4387.
61. W. Shi, J. Zhu, D. H. Sim, Y. Y. Tay, Z. Lu, X. Zhang, Y. Sharma, M. Srinivasan, H. Zhang and H. H. Hng, *J. Mater. Chem.*, 2011, 21, 3422-3427.
62. P. Gifford, J. Adams, D. Corrigan and S. Venkatesan, *J. Power Sources*, 1999, 80, 157-163.
63. Y. Wang, Z. Shi, Y. Huang, Y. Ma, C. Wang, M. Chen and Y. Chen, *J. Phys. Chem. C*, 2009, 113, 13103-13107.
64. F. Xu, R. Cai, Q. Zeng, C. Zou, D. Wu, F. Li, X. Lu, Y. Liang and R. Fu, *J. Mater. Chem.*, 2011, 21, 1970-1976.
65. Jaidev, R. I. Jafri, A. K. Mishra and S. Ramaprabhu, *J. Mater. Chem.*, 2011, 21, 17601.
66. N. Brun, S. R. Prabaharan, C. Surcin, M. Morcrette, H. Deleuze, M. Birot, O. Babot, M.-F. Achard and R. Backov, *J. Phys. Chem. C*, 2011, 116, 1408-1421.
67. X. Li and B. Wei, *Nano Energy*, 2012, 1, 479-487.